# Numerical Simulation of Powder Flow and Laser-Substrate Interaction in a Multi-Channel Coaxial Nozzle DMD Process

**D. Chatterjee**
*Advance Design Analysis Group, CSIR-CMERI, Durgapur, West Bengal*
*Email : d_chatterjee@cmeri.res.in*

**P. Pant, S. Samanta, A.K. Lohar**
*Near-Net Shape Manufacturing Technology, CSIR-CMERI, Durgapur, West Bengal*

**Titas Nandi**
*Department of Mechanical Engneering, Jadavpur University, Kolkata-700032*

**ABSTRACT**

Direct Metal Deposition (DMD) is a form of an additive manufacturing (AM) process which promises to deliver end-user product. DMD is used for rapid prototyping, fabrication, surface modification and repair of components. A layer by layer deposition of powder material on a melt pool over a substrate is created by coaxial fed laser beam under a controlled monitoring of melt pool temperature to create a fully functional prototype directly from a CAD design.

The process of direct metal deposition involves some of the complex phenomena like powder flow through the nozzle, formation of powder stream, laser-powder interaction, laser-substrate interaction, powder-melt pool interaction, the flow of melt pool etc. This study deals with the powder flow model and the evolution of the melt pool geometry which are significantly important to obtain the powder efficiency.

This article represents a physical-computational model to describe the powder stream dynamics and melt pool formation in DMD process. Numerical simulations are performed using Ansys FLUENT software. The computational domain consists of the nozzle geometry and the region beneath the nozzle for powder flow dynamics and substrate region for melt pool dynamics. The model is successful in predicting the distance suitable for substrate placement, powder distribution at the position of convergence of powder streams and melt pool geometry. The ideal substrate position of 11-14 mm beneath the nozzle and Gaussian powder stream distribution are determined from the powder flow model, while the melt pool diameter comparable to the size of the laser beam is identified. Using the models developed, powder efficiency is obtained which is a function of the melt pool radius and the radius corresponding to the maximum powder number concentration.

**Keywords:** direct metal deposition, numerical simulation, CFD, Fluent;

## INTRODUCTION

Last three decades had seen additive manufacturing (AM) as an emerging technology which offers several advantages over conventional methods like sustainability, complexity in design, zero lead time, portable manufacturing and almost nil intermediate process. Still, this technology is in its infancy and developments are in progress with the expanding scope of this technology in different fields of interests. AM techniques require much less machining than traditional castings or forging processes by only adding material where required, thus offering weight saving. The AM process had gained significant importance in the fields but are not limited to automobile, aerospace manufacturing and also in jewelry, biomedical and electronic manufacturing industries[1].

During the laser deposition, the powder is transported by a gas flow through a conical coaxial nozzle to the laser beam and substrate. Powder flow should be ascertained to converge at an appropriate distance from the nozzle so as to utilize the maximum powder transported in that region[2]. Yang[3] proposed a model to predict the maximum powder stream concentration in coaxial laser cladding for different powder properties, nozzle geometries and shielding gas settings. Lin[4] simulated the powder flow structures of a coaxial nozzle for laser cladding by the

numerical program FLUENT with various arrangements of the nozzle exit.

Wen and Shin[5] modelled the melt pool process incorporating the Marangoni and capillary effects, and used a level-set method for melt pool surface tracking. Pinkerton[6] considered only conduction as heat losses to the melt pool. It assumed the simplified case of a moving point heat source on a semi-infinite substrate. A subroutine for the geometry modelling was written in MATLAB. Khajepour[7] developed a model for simulating the real-time melt-pool shape and geometries and predicted the local solidification conditions along the solid/liquid interface using element activation/ deactivation in each solution time step.

The objective of the present research is to determine the deposition efficiency in a direct metal deposition process using a multi-channel coaxial nozzle powder delivery. For this, the study is divided into two modules, the powder flow and the melt pool model respectively. From powder flow model, the powder concentration, powder distribution for different powder particle size is determined at a certain stand-off distance from the nozzle exit. The diameter of melt pool created as a result of heating from a Gaussian distributed laser source is obtained from the melt pool model. Later, a relation from previous literature is used to determine the powder deposition efficiency which is a function of powder flow diameter and melt pool diameter.

## NUMERICAL MODELLING

### Powder Flow Model

#### Problem Geometry and Boundary Conditions:

A schematic of the coaxial powder delivery nozzle deposition mechanism is shown in Fig. 1. In this model, the substrate is stationary in a three-dimensional Cartesian coordinate. A focused laser beam in negative Y direction strikes the substrate which is kept at an identified stand-off distance. The whole nozzle assembly moves in the negative X direction with a scanning speed of $U_{scan}$. The computational domain consists of nozzle and space beneath the nozzle for powder flow model. The powder is delivered using a powder feeder. The flow converges at a specified stand-off distance from the nozzle. The laser beam is coaxially fed which when irradiates a small region of the substrate creates a molten pool. Thus a deposition layer is formed as a result of melting and solidification by continually moving laser beam and powder material feeding. To study the CFD model a quarter nozzle is considered due to the symmetric features as shown in Fig. 2. The CAD model is then meshed using the ICEM CFD tool. The hybrid mesh consisting of tetra and prism elements are used. The region below the nozzle is of dimensions $15 \times 25 \times 15$ ($mm^3$).

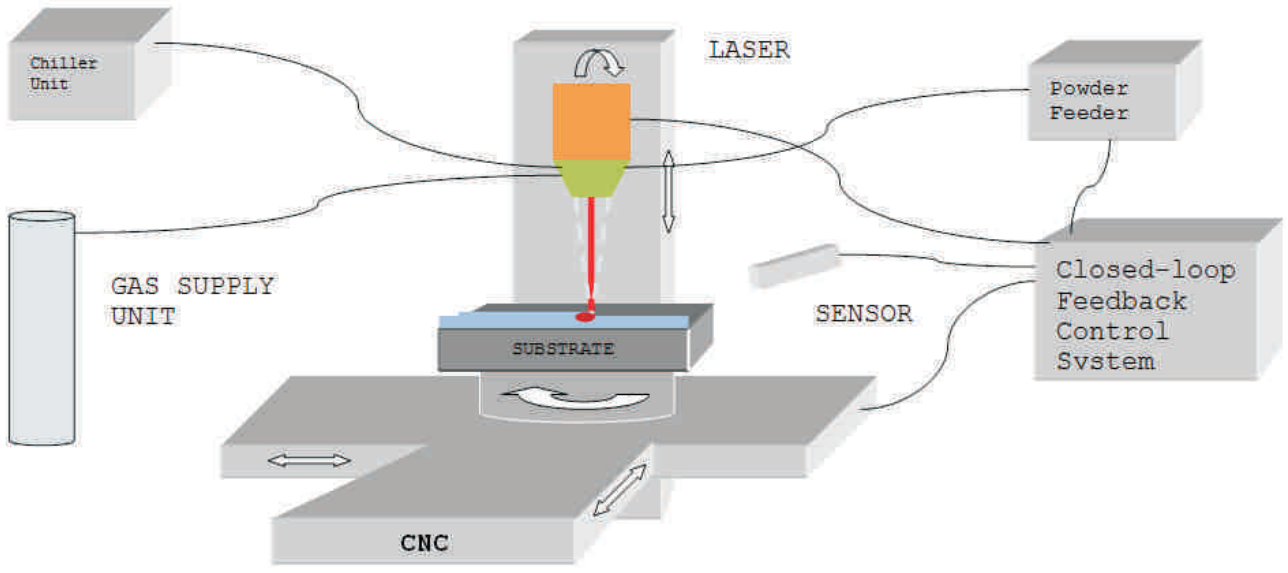


Fig.1 Direct metal deposition system and its components

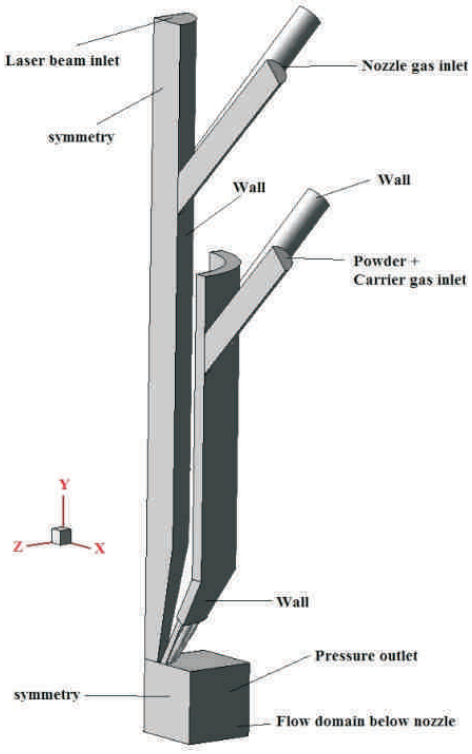


Fig.2 Representation of quarter symmetric nozzle with boundary conditions

Assumptions and boundary conditions:

- For gas atomized particles shape factor = 0.8 is considered
- Argon is considered as the carrier gas and centre nozzle gas
- Surface injection method of particle is considered.

The powder particle-gas flow simulation is studied using a combined Lagrangian-Eulerian approach wherein the powder particles are treated as dispersed phase in a continuous gas phase. Time averaged governing equation for turbulent flow are expressed as

Conservation of mass:

$$\frac{\partial(\rho u_i)}{\partial x_i} = 0 \qquad \text{..... Equation 1}$$

where ρ is the gas density and the vectors $u_i$ and $x_i$ prepresents the velocity and position, respectively.

Conservation of momentum:

$$\frac{\partial}{\partial x_j}(\rho u_i u_j) = -\frac{\partial \rho}{\partial x_i} + \frac{\partial \tau_{ij}}{\partial x_j} + \rho g_i$$

..... Equation 2

where p is the pressure, g is the gravitational acceleration and $\tau_{ij}$ is the viscous stress tensor defined by

$$\tau_{ij} = \left[(\mu + \mu_t)\left(\frac{\partial u_i}{\partial x_j} + \frac{\partial u_j}{\partial x_i}\right)\right] - \frac{2}{3}\mu_t \frac{\partial u_i}{\partial x_i}\delta_{ij}$$

..... Equation 3

where μ is the molecular viscosity and $\delta_{ij}$=1 for $i$=$j$ otherwise $\delta_{ij}$=0 and $\mu_t$ is the turbulent viscosity defined by

$$\mu_t = \rho C_\mu \frac{k^2}{\varepsilon} \qquad \text{..... Equation 4}$$

where $c_\mu$ is the constant and usually taken as 0.09, $k$ is the kinetic energy of turbulence and ε is the dissipation rate of kinetic energy, which are defined through the k-ε turbulence model.

Conservation of kinetic energy:

$$\frac{\partial}{\partial x_i}(\rho k u_i) = \frac{\partial}{\partial x_j}\left[\left(\mu + \frac{\mu_t}{\sigma_k}\right)\frac{\partial k}{\partial x_j}\right] + G_k + G_b - \rho\varepsilon$$

..... Equation 5

Conservation of dissipation rate of kinetic energy:

$$\frac{\partial}{\partial x_i}(\rho\varepsilon u_i) = \frac{\partial}{\partial x_j}\left[\left(\mu + \frac{\mu_t}{\sigma_\varepsilon}\right)\frac{\partial \varepsilon}{\partial x_j}\right] + C_{1\varepsilon}\frac{\varepsilon}{k}(G_k + G_b) - C_{2\varepsilon}\rho\frac{\varepsilon^2}{k}$$

..... Equation 6

$$G_b = -g_i \frac{\mu_t}{\rho \Pr_t}\frac{\partial p}{\partial x_i} \qquad \text{..... Equation 7}$$

$$G_k = \mu_t\left(\frac{\partial u_i}{\partial x_j} + \frac{\partial u_j}{\partial x_i}\right)\frac{\partial u_i}{\partial x_j} \qquad \text{..... Equation 8}$$

where $C_1$=1.44, $C_{2\varepsilon}$=1.92,$\sigma_k$=1.0 and $\sigma_\varepsilon$=1.3 are empirical constants, $Pr_t$ is the turbulent Prandtl number, $G_k$ is the generation of turbulence kinetic energy due to the mean velocity gradients, and $G_b$ is the generation of turbulence kinetic energy due to buoyancy.

## Particle-gas momentum exchange:

A force balance equation to model powder particles in the discrete phase model (DPM) is used to determine the trajectory of the powder particles.

$$\frac{du_p}{dt} = F_D(u - u_p) + g_x\left(\frac{\rho_p - \rho}{\rho_p}\right) + F_x$$

..... Equation 9

where is the particle velocity, $u$ is the phase field velocity, ρ is the fluid density, $\rho_p$ is the density of powder particle. $F_D$

can be calculated using eq.(10) as

$$F_D = \frac{18\mu}{\rho_p d_p^2}\frac{C_D Re}{24}$$ ..... Equation 10

where $\mu$, the fluid phase dynamic viscosity, and *Re* is the Reynolds number expressed in Eq.(11)

$$F_D = \frac{18\mu}{\rho_p d_p^2}\frac{C_D Re}{24}$$ ..... Equation 11

The drag coefficient, with four empirical constants to incorporate the non-spherical nature of the particles is given as

$$C_D = a_1 + \frac{a_2}{Re} + \frac{a_3}{Re}$$ ..... Equation 12

where $a_1$,$a_2$,and $a_3$ are empirical constants. The discrete random walk model as used by Tabernero.et.al[8] is applied.

### Process Parameters:

To obtain the following objective a set of process parameters like powder mass flow rate (P.F.R), carrier gas flow rate (C.G.F.R) and mean particle diameter (M.P.D) has been chosen under the machine specifications which are given below in the following Table 1. The nozzle gas flow rate (N.G.F.R) is kept constant at 10 L/min. The powder study assumes the AISI316 particles having density of 7800 kg/m$^3$.

### Numerical Procedure:

Equations for powder flow are solved using Ansys Fluent, version 13.0. The discretization scheme used is second order upwind for momentum and turbulence equations, and SIMPLEC scheme for pressure-velocity coupling. The equations are solved using the segregated solver. As the governing equations are non-linear and coupled, several iterations of the solution loop are performed before a converged solution is obtained. The convergence criteria for all simulations were $10^{-6}$.

Table 1.Process parameters and their levels for powder flow model

| Process Parameters | Levels | | |
|---|---|---|---|
| | 1 | 2 | 3 |
| Powder mass flow rate (g/min) | 5 | 10 | 15 |
| Carrier gas flow rate (L/min)5 | 7.5 | 10 | |
| Mean powder particle diameter(µm) | 40 | 60 | 80 |

## MELT POOL MODEL

### Problem Geometry and Boundary Conditions:

The melt pool model study considers the substrate region having size 8mm × 8mm × 4mm. The high density laser beam of Gaussian distribution is focused at the focal position over the substrate top. This high energy laser beam initially transfers the heat to substrate using conduction phenomenon. Later, a melt pool is formed and convection phenomenon dominates. A 1kW laser of diameter 0.6 mm diameter is considered for the present study. The AISI316 material substrate is used in present case[9].

Following consideration were made in developing melt pool model:

1. The flow is laminar and incompressible
2. The laser beam distribution is Gaussian
3. Temperature dependent properties for thermal conductivity, viscosity are considered.

An enthalpy-porosity technique is used for modeling the melting process. In this technique, the melt interface is not tracked explicitly. Instead, a quantity called the liquid fraction based on enthalpy balance indicates the fraction of cell volume that is in liquid form, is associated with each cell in the domain[10].

The enthalpy of the material is computed as the sum of the sensible enthalpy, *h* and the latent heat,

$$H = h + \Delta H$$ ..... Equation 13

Where $h = h_{ref} + \int_{T_{ref}}^{T} c_p dT$ ..... Equation 14

$$\beta = 0 \quad \text{if} \quad T < T_{solidus}$$ ..... Equation 15

$$\beta = 1 \quad \text{if} \quad T > T_{liquidus}$$ ..... Equation 16

$$\beta = \frac{T - T_{solidus}}{T_{liquidus} - T_{solidus}} \quad \text{if} \quad T_{solidus} < T < T_{liquidus}$$ ..... Equation 17

The latent heat content can now be written in terms of latent heat of the material, *L*:

$$\Delta H = \beta L \quad \text{..... Equation 18}$$

$$\frac{\partial}{\partial t}(\rho H) + \nabla.(\rho \vec{v} H) = \nabla.(k \nabla T) + S \quad \text{..... Equation 19}$$

Where H ρ v s are enthalpy, density, fluid velocity and source term respectively. The enthalpy-porosity model for solidification treats the mushy region as a porous medium. The porosity in each cell is set equal to the liquid fraction in that cell. In fully solidified regions, the porosity is equal to zero, which extinguishes the velocity in this region. The momentum sink due to reduced porosity in mushy zone takes the following form:

$$S = \frac{(1-\beta)^2}{(\beta^3+\chi)} A_{mush} \vec{v} \quad \text{..... Equation 20}$$

Where β is the liquid volume fraction, χ is a small number (0.001) to prevent division by zero, and is the mushy zone constant.

Beside the dominant influence of the heat conduction, the heat losses by convection and radiation are included in thermal analysis, and are incorporated as boundary conditions for specific areas. An enhanced heat transfer coefficient,used by Goldak[11] which combines the radiative and convective heat transfer coefficient is used in the present study. Considering Gaussian heat input and a combined convective and radiative heat loss, the boundary at top of substrate where laser is irradiated can be represented in the following form:

$$-k\frac{\partial T}{\partial y} = -q^{"}(r) \quad h_c(T - T_\infty) \quad + \quad \text{..... Equation 21}$$

WHERE,

$$h_c = 24.1 \times 10^{-4} \epsilon_p T^{1.61} \quad \text{..... Equation 22}$$

and

$$\mathbf{q^{"}(r) = \frac{\varepsilon_0 P}{\pi r_q^2} \exp\left(\frac{-r}{r_q^2}\right)} \quad \text{..... Equation 23}$$

AND AT THE REGION AT TOP OTHER THAN IRRADIATED ONE IS:

$$\mathbf{-k\frac{\partial T}{\partial y} = h_c(T - T_\infty)} \quad \text{..... Equation 24}$$

Whereas for side faces and bottom face insulated thermal boundary condition is used

$$\frac{\partial T}{\partial y} = 0 \quad \text{..... Equation 25}$$

### CALCULATION FOR POWDER EFFICIENCY:

POWDER EFFICIENCY[12] is a function of the powder stream radius at stand-off distance and the size of melt pool. Since the melt pool size is similar to the laser spot diameter for the given set of parameters[13] the powder stream radius is calculated for different pair of parameters and is related to obtain the powder efficiency from the relation shown in eq. 26.

$$\eta_P = 1 - exp\left(\frac{-2r_m^2}{r_P^2}\right) \quad \text{..... Equation 26}$$

## RESULTS AND DISCUSSION

### Powder flow study

#### Stand-off Distance:

Figure.3 depicts the variation of the powder concentration at various planes beneath the nozzle tip. Since the substrate should be placed at a distance of maximum powder concentration, it can be seen that a range of 11-14 mm is found to be suitable for the given set of parameters.

#### Powder concentration diameter:

During the flow along the stream the powder particles structure can be divided into three regimes: converging stream, waist region and diverging stream as shown in fig. 4. At this waist region the core diameter of the stream is determined. The powder distribution in this region is nearly gaussian. This core diameter is determined from post processing.

The simulated result for powder flow is verified experimentally using a high speed camera. The

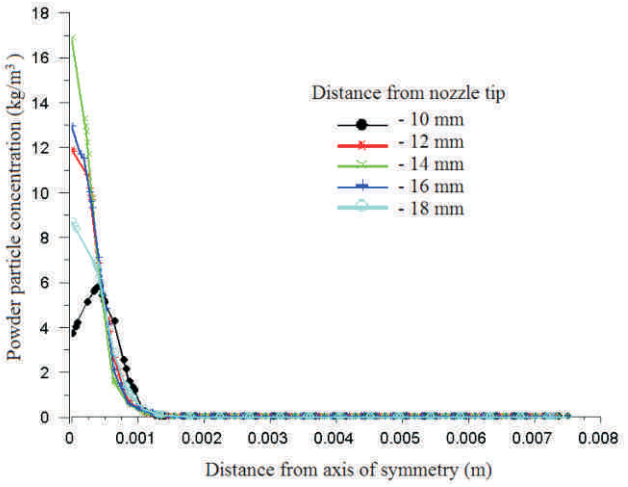


Fig.3 powder concentration and focusing diameter at various planes

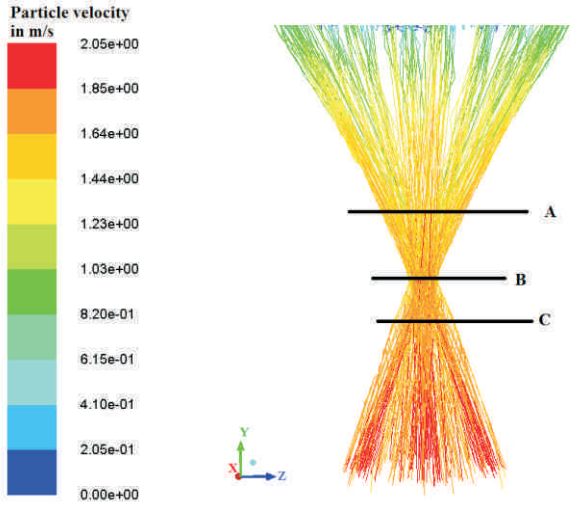


Fig.4 particle trajectory and velocity beneath the nozzle tip

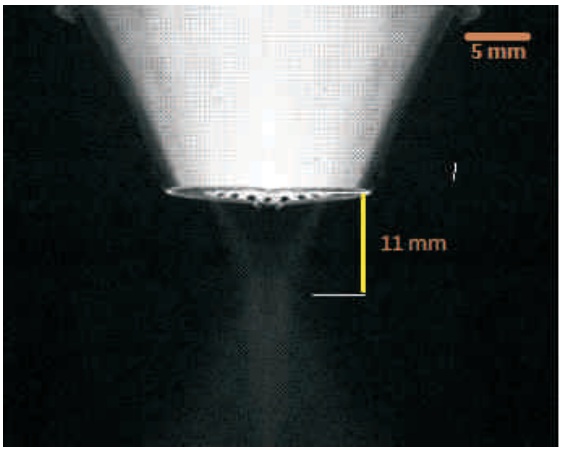


Fig. 5 experimental result of powder flow study beneath the nozzle

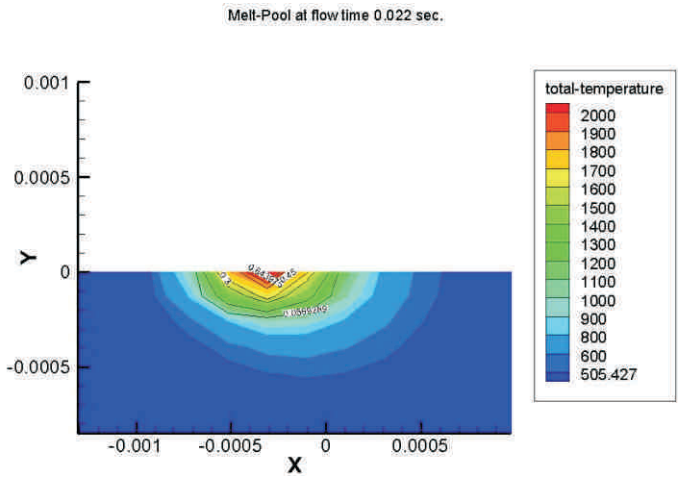


Fig.6 contours of temperature at substrate with streamlines Of velocity (laser power= 600w)

experimental result reveals that the powder converges at 11mm from the nozzle tip which is in accordance with the simulations performed. The powder flow image (fig. 5) shows the convergence, waist and spread of powder stream.

## *MELT POOL STUDY*

This study describes the melting of substrate material on interaction with high intensity laser beam and scanning of laser beam in absence of the powder flow. Figure.6 shows the melt pool variation with the scanning speed .the elliptical profile of beam scanning forms a tail like shape as beam progresses towards negative x direction, it can be seen that due to the effect of moving laser, surface fluid will flow backward, and form a melt pool tail.

The melt pool width obtained from simulation is equal to the diameter of the illuminated beam, as shown in figure. 7. The results are in good agreement with the previous work performed. The liquid fraction of 1 obtained is the result of the temperature above the melting point predicts the measure of the melt pool depth created. The maximum temperature obtained a point over substrate during laser scanning speed of 4mm/sec is 3420k (as seen in fig. 8). It can be helpful in determining the cooling rate.

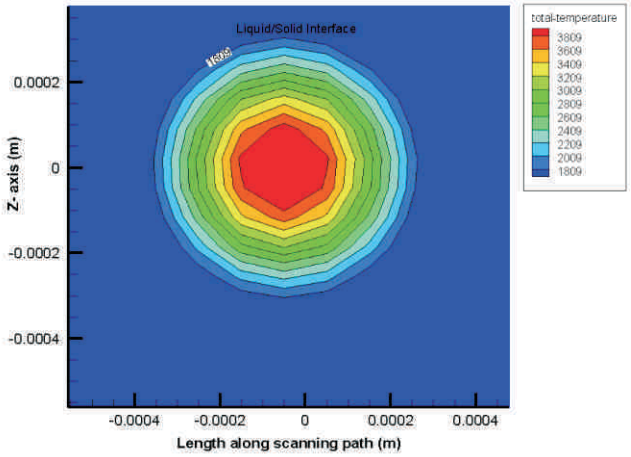


Fig.7 contours of temperature at substrate depicting

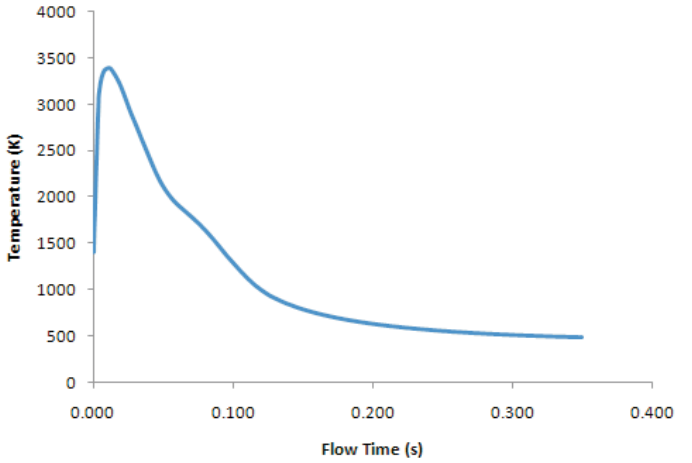


Fig. 8 maximum temperature obtained at scanning

## CONCLUSION

In this work, a numerical model is developed to analyze the powder flow behavior and melt pool dynamics in laser based direct metal deposition system. This model predicts the powder distribution at stand-off distance, converging distance of powder flow and powder particle trajectory inside and in the domain below nozzle tip. The simulated melt pool diameter is same as the laser beam irradiated diameter. The powder efficiency in the present study obtained from an empirical relation is found as 51%. Thus the process of metal deposition promises a better scope for the repair of dies and moulds, which will save the idle time, additional costs during malfunctioning in a foundry.

## ACKNOWLEDGEMENT

This work is financially supported by dst (govt. Of india) through the grant-in-aid project no. Gap 121512.

## REFERENCES

1. Thompson, S. M. and Shamshei N. et.al, An overview of direct laser deposition for additive manufacturing: Part 1: Transport phenomena modelling and diagnostics, Additive Manufacturing, 2015, Vol.8, p. 36-62.

2. Zekovic S., Dwivedi R. and Kovacevic R., Numerical simulation and experimental investigation of gas-powder flow from radially symmetrical nozzles in laser-based direct metal deposition, International Journal of Machine Tools and Manufacture, 2007, Vol. 47(1), p. 112-123.

3. Yang, N., Concentration model based on movement model of powder flow in coaxial laser claddin, Optics and Laser Technology, 2009, Vol. 41, p. 94-98.

4. Lin, J., Numerical simulation of the focused powder streams in coaxial laser cladding, Journal of Material Processing Technology, 2000, Vol. 105, p.17–23.

5. Wen, S. Y. and Shin, Y. C., Modelling of transport phenomena during the coaxial laser direct deposition process, J. Appl. Phys. Vol. 108, 2010, p. 044908.

6. Pinkerton, A. and Li, L., Modelling the geometry of a moving laser melt pool and deposition track via energy and mass balances, J. Phys. D: Appl. Phys., 2004, Vol. 37, p.1885–1895.

7. Fathi, E. and Toyserkani, A. Khajepour, and M. Durali, Prediction of melt pool depth and dilution in laser powder deposition, J. Phys. D, 2006, Vol. 39, p. 2613–2623.

8. Tabernero et.al, Numerical simulation and experimental validation of powder flux distribution in coaxial laser cladding, Journal of Material Processing Technology, 2010, Vol. 210, p. 2125–2134.

9. Ibarra-Medina, J. and Pinkerton, A. J., A CFD model of the laser, coaxial powder stream and substrate interaction in laser cladding, Physics Procedia, 2010, Vol. 5, p. 337–346.

10. Fluent Inc., FLUENT 13.0, User Guide, 2010.

11. Goldak, J., Chakravarti, A. and Bibby M., A new finite element model for welding heat sources, Metallurgical Transactions B, 1984, Vol.15B, p. 299-305.

12. Liu, J. and Li, L., Effects of process variables on laser direct formation of thin wall, Opt. Laser Technology, 2007, Vol. 39, p. 231–236.

13. Choi, J. and Chang, Y., Analysis of Laser Control effects for direct metal deposition process, J. of Mechanical Science and Technology, 2006, Vol. 20, p. 1680-1690.